Identification of geometric parameters influencing the flow-induced vibration of a two-layer self-oscillating computational vocal fold model

Brian A. Pickup and Scott L. Thomson[a)]
Department of Mechanical Engineering, Brigham Young University, Provo, Utah 84602

(Received 22 June 2010; revised 19 January 2011; accepted 25 January 2011)

Simplified models have been used to simulate and study the flow-induced vibrations of the human vocal folds. While it is clear that the models' responses are sensitive to geometry, it is not clear how and to what extent specific geometric features influence model motion. In this study geometric features that played significant roles in governing the motion of a two-layer (body-cover), two-dimensional, finite element vocal fold model were identified. The model was defined using a flow solver based on the viscous, unsteady, Navier–Stokes equations and a solid solver that allowed for large strain and deformation. A screening-type design-of-experiments approach was used to identify the relative importance of 13 geometric parameters. Five output measures were analyzed to assess the magnitude of each geometric parameter's effect on the model's motion. The measures related to frequency, glottal width, flow rate, intraglottal angle, and intraglottal phase delay. The most significant geometric parameters were those associated with the cover—primarily the pre-phonatory intraglottal angle—as well as the body inferior angle. Some models exhibited evidence of improved model motion, including mucosal wave-like motion and alternating convergent-divergent glottal profiles, although further improvements are still needed to more closely mimic human vocal fold motion. © *2011 Acoustical Society of America*. [DOI: 10.1121/1.3557046]

PACS number(s): 43.70.Aj, 43.70.Bk [DAB] Pages: 2121–2132

I. INTRODUCTION

Voice production is the result of the flow-induced vibration of the vocal folds. Simplified, self-oscillating continuum-type synthetic models of the vocal folds have been used to study various aspects of this system, such as aerodynamic energy transfer (Thomson *et al*., 2005), coupling of subglottal acoustics with vocal fold models (Zhang *et al*., 2006a), acoustically and aerodynamically driven modes of vibration (Zhang *et al*., 2006b; Zhang *et al*., 2009), glottal airflow (Neubauer *et al*., 2007; Drechsel and Thomson, 2008), material asymmetries (Pickup and Thomson, 2009), flow-structure-acoustic interactions (Becker *et al*., 2009), and subglottal flow (Misun *et al*., 2011). Synthetic models such as these are inexpensive, durable, relatively easy to fabricate, and conveniently parameterized. These features allow for detailed parametric investigations of the underlying flow-induced vibration physics.

While these models have demonstrated some vibratory similarities with those of the human vocal folds, such as with regards to onset pressure, frequency, and amplitude, some models have also exhibited a few aspects of less-than-life-like motion-related behavior. Examples include the lack of mucosal wave-like motion (a key feature of phonation, Bless *et al*., 1987), excessive inferior-superior motion (Drechsel and Thomson, 2008), and a generally divergent profile during vibration (as opposed to the more realistic convergent-divergent profile) (Pickup and Thomson, 2010). It is therefore desirable to understand the relationship between the models' various geometric and material characteristics and their flow-induced responses.

Researchers have studied how geometric parameters and material properties influence the resulting fluid, solid, and/or coupled fluid–solid dynamics of vocal fold models. For example, static models have been used to study intraglottal pressure and flow characteristics. One example is the "M5" static vocal fold model of Scherer *et al*. (2001a), which has been used to investigate the effect of asymmetric intraglottal profiles on intraglottal pressure distributions. By using the same model, Scherer *et al*. (2001b) found that the intraglottal pressure distribution was dependent upon the curvature of the exit radius in models with convergent intraglottal profiles. Li *et al*. (2006) numerically investigated the influence of inferior and superior surface angles of these static models. They showed that intraglottal pressures are relatively insensitive to inferior and superior vocal fold surface angles, although they emphasized the need to further study how these angles might influence vocal fold motion.

Studies on the effects of vocal fold thickness, epithelial membrane thickness, pre-phonatory glottal geometry, and cover layer material properties on phonation threshold pressure have been investigated using membrane-type synthetic vocal fold models. Titze *et al*. (1995) studied the effects of cover layer material properties and pre-phonatory glottal width on phonation threshold pressure of a physical model. They showed that phonation threshold pressure increases with increasing pre-phonatory glottal width. By using a similar model, Chan *et al*. (1997) showed that phonation threshold pressure increases with non-zero pre-phonatory glottal

[a)]Author to whom correspondence should be addressed. Electronic mail: thomson@byu.edu

convergence angles, increased epithelial membrane thickness, and decreased vertical model thickness. These studies did not include analysis of model motion.

Continuum-based numerical vocal fold models have also been studied in order to understand model response characteristics. Cook and Mongeau (2007) investigated the role of lateral depth, anterior–posterior length, and vertical thickness of a single-layer, three-dimensional vocal fold model on modal frequencies. They showed that modal frequencies were most sensitive to variations in anterior–posterior length and least sensitive to changes in vertical thickness. Subsequently, Cook *et al*. (2009) extended this study to consider how other geometric and material parameters influenced the modal response of a three-dimensional body-cover layer computational model. These two studies focused on *in vacuo* modal analysis, absent flow-induced vibration. Zhang (2009) used a two-layer body-cover continuum-based vocal fold model with a reduced-order flow model to study mechanical and geometric properties on model response at phonation onset. It was shown that significant changes in phonation onset frequency can be induced by slight changes in body layer stiffness and that similar changes in phonation onset frequency may also be induced by geometric changes.

Pickup and Thomson (2010) recently compared the flow-induced responses of synthetic models with geometries based on magnetic resonance imaging (MRI) data with the responses of models based on the more geometrically simplified M5-based model. The MRI-based models showed evidence of mucosal wave-like motion, a feature absent in the M5-based physical models. The M5-based model also showed primarily divergent motion, whereas convergent-divergent motion was evident in the MRI-based models. The M5-based model pre-phonatory intraglottal profiles were straight and it was hypothesized that convergent pre-phonatory profiles may have played a significant role in the improved convergent-divergent behavior of the MRI-based model. It was concluded that parametric studies investigating the role of the various geometric features on the flow-induced response was necessary.

The research in this paper was undertaken to determine which geometric features significantly influence a vocal fold model's flow-induced vibratory response. The model (see Fig. 1) was a modification of the M5 model of Scherer *et al*. (2001a). This was chosen because it (or a very similar representation) has been used in several recently reported studies, and in some of these reports, it has been emphasized that improvements to the model motion are needed in order to better represent vocal fold motion (e.g., Zhang *et al*., 2006a,b; Drechsel and Thomson, 2008; Zhang *et al*., 2009; Pickup and Thomson, 2009, 2010). This work is also closely related to that of Cook and Mongeau (2007), Cook *et al*. (2009), and Zhang (2009), in that a similarly defined two-dimensional computational vocal fold model was used, only the present work considers a model in which the motion was fully coupled with a Navier–Stokes-based flow solver. In this work, the model geometry generally consisted of linear subglottal and supraglottal profiles of varying angles, a linear intraglottal profile of varying angle and length, and rounded

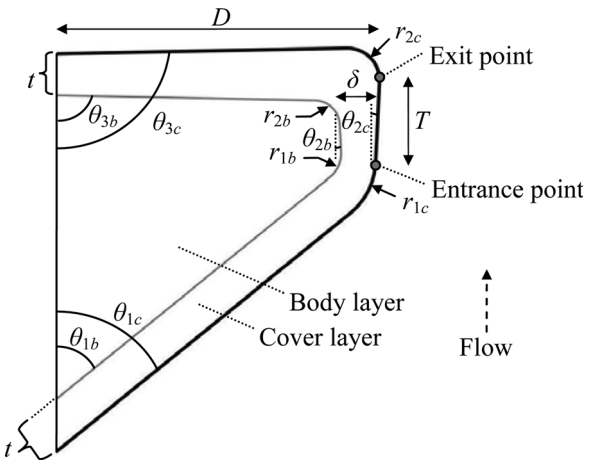

FIG. 1. Parametric two-layer vocal fold model.

glottal inlet and exit regions of varying radii. A body-cover representation was used, with body and cover geometries independently defined. In order to accommodate the significant computation times required for model simulation, the geometric parameters were defined and the simulation results were analyzed based on a screening-type design-of-experiments methodology. The simulation results were analyzed to estimate the relative significance of different geometric parameters on the model's response.

In the following sections, the computational approach is described, including model parameterization, screening design, numerical methods, and data analysis. The results, including rankings of the influence of model parameters on various aspects of model response, are presented and discussed. Finally, suggestions for further studies of specific model parameters and development of improved models are provided.

II. METHODS

A. Model definition and parameterization

The model body and cover layer geometries were defined using 14 parameters (see Fig. 1). Of these the model depth, *D* (the maximum depth from the medial edge to the lateral edge), was constant and the other 13 were variable. The variable parameters were each given a low, baseline, and high value (see Table I), according to similar values found in previous reports (Stiblar-Martincic, 1997; Scherer *et al*., 2001a; Tayama *et al*., 2002; Agarwal *et al*., 2003; Nanayakkara, 2005; Sidlof *et al*., 2008). It is noted that variations in the parameters resulted in the base vertical thickness dimension (corresponding to the fixed, lateral edge length; i.e., that of the leftmost vertical edge in Fig. 1) ranging from 10 to 11.2 mm.

B. Screening design

In order to determine which geometric parameters were significant in terms of influencing model response, a 20-run Plackett–Burman screening design-of-experiment was used to analyze the effect of the 13 variable parameters on various measurements of model motion. This approach, as opposed

TABLE I. Vocal fold model geometric parameter values and descriptions.

Parameter	Baseline	Low/high values	Description
θ_{1c}, θ_{1b}	50°	49.35, 50.65°	Inferior glottal angle (cover, body)
θ_{2c}, θ_{2b}	0°	−2.75, 2.75°	Intraglottal angle (− divergent, + convergent) (cover, body)
θ_{3c}, θ_{3b}	90°	88.85, 91.15°	Superior glottal angle (cover, body)
r_{1c}	1.5 mm	1.18, 1.82 mm	Entrance radius (cover)
r_{1b}	1.12 mm	0.80, 1.45 mm	Entrance radius (body)
r_{2c}	0.987 mm	0.837, 1.137 mm	Exit radius (cover)
r_{2b}	0.513 mm	0.36, 0.66 mm	Exit radius (body)
T	2.0 mm	1.85, 2.15 mm	Distance between glottal entrance and exit points
Δ	1.15 mm	1.0, 1.3 mm	Maximum medial cover layer thickness
T	1.15 mm	1.075, 1.225 mm	Inferior and superior cover layer thickness
D	8.4 mm	8.4 mm	Maximum lateral distance from medial edge to lateral edge

to a full-factorial design-of-experiment or sensitivity analysis, was taken because of the computational cost of the model simulations (approximately 19 h per simulation on a 2.8 GHz quad-core Intel Nehalem CPU; time to complete all cases was reduced by running simulations simultaneously on a supercomputer). The combinations of high-low parameter values for each simulation were adapted from Lawson and Erjavec (2001) and are given in Table II. Since 13 geometric attributes were analyzed but 20 runs were performed, six unassigned factors (X14–X19 in Table II) represent unknown combinations of second, third, and higher-order interactions of the 13 assigned parameters. In addition to the 20 high-low runs, an additional run with all parameters set to baseline values was executed.

The benefit of using a Plackett–Burman design is that the influence of each parameter on the measured output can be estimated using relatively few runs. The tradeoff is that interactions between parameters are confounded with the main effect of each parameter. It is therefore intended to serve as a screening design to be followed up with focused, more detailed studies on the parameters found to be significant. In this study, analysis of each parameter's effect was used to determine which parameters are recommended for such future detailed studies.

The levels of the high and low parameter values were chosen such that changing each parameter from low to high resulted in a similar overall change (in terms of magnitude) in the model's shape. For example, the inferior surface angle (θ_{1c}) levels were determined as follows. First, all parameters were set to their baseline values. Then, keeping all other parameters at their baseline values, high and low θ_{1c} values that yielded 0.15 mm displacement of a point on the glottal entrance radius position from its original position were determined (yielding a total displacement of 0.3 mm of the

TABLE II. Plackett–Burman 20-run statistical design-of-experiment table. "1" indicates a high geometric value; "−1" indicates a low geometric value. In row 1, factors X1 through X13 correspond to model variable parameters denoted directly underneath in row 2. Factors X14 through X20 represent unknown interactions of main factors. Run 0 corresponds to the baseline set of parameter values.

Run	X1 r_{1c}	X2 r_{1b}	X3 r_{2c}	X4 r_{2b}	X5 θ_{1c}	X6 θ_{1b}	X7 θ_{2c}	X8 θ_{2b}	X9 θ_{3c}	X10 θ_{3b}	X1 T	X2 δ	X3 t	X14 X14	X15 X15	X16 X16	X17 X17	X18 X18	X19 X19
0	0	0	0	0	0	0	0	0	0	0	0	0	0	0	0	0	0	0	0
1	1	1	−1	−1	1	1	1	1	−1	1	−1	1	−1	−1	−1	−1	1	1	−1
2	1	−1	−1	1	1	1	1	−1	1	−1	1	−1	−1	−1	−1	1	1	−1	1
3	−1	−1	1	1	1	1	−1	1	−1	1	−1	−1	−1	−1	1	1	−1	1	1
4	−1	1	1	0.2	1	−1	1	−1	1	−1	−1	−1	−1	1	1	−1	1	1	−1
5	1	1	1	1	−1	1	−1	1	−1	−1	−1	−1	1	1	−1	1	1	−1	−1
6	1	1	1	−1	1	−1	1	−1	−1	−1	−1	1	1	−1	1	1	−1	−1	1
7	1	1	−1	1	−1	1	−1	−1	−1	−1	1	1	−1	1	1	−1	−1	1	1
8	1	−1	1	−1	1	−1	−1	−1	−1	1	1	−1	1	1	−1	−1	1	1	1
9	−1	1	−1	1	−1	−1	−1	−1	1	1	−1	1	1	−1	−1	1	1	1	1
10	1	−1	1	−1	−1	−1	−1	1	1	−1	1	1	−1	−1	1	1	1	1	−1
11	−1	1	−1	−1	−1	−1	1	1	−1	1	1	−1	−1	1	1	1	1	−1	1
12	1	−1	−1	−1	−1	1	1	−1	1	1	−1	−1	1	1	1	1	−1	1	−1
13	−1	−1	−1	−1	1	1	−1	1	1	−1	−1	1	1	1	1	−1	1	−1	1
14	−1	−1	−1	1	1	−1	1	1	−1	−1	1	1	1	1	−1	1	−1	1	−1
15	−1	−1	1	1	−1	1	1	−1	−1	1	1	1	1	−1	1	−1	1	−1	−1
16	−1	1	1	−1	1	1	−1	−1	1	1	1	1	−1	1	−1	1	−1	−1	−1
17	1	1	−1	1	1	−1	−1	1	1	1	1	−1	1	−1	1	−1	−1	−1	−1
18	1	−1	1	1	−1	−1	1	1	1	1	−1	1	−1	1	−1	−1	−1	−1	1
19	−1	1	1	−1	−1	1	1	1	1	−1	1	−1	1	−1	−1	−1	−1	1	1
20	−1	−1	−1	−1	−1	−1	−1	−1	−1	−1	−1	−1	−1	−1	−1	−1	−1	−1	−1

point position when alternating between high and low settings of parameter θ_{1c}). This was repeated for all parameters. The total displacement value of 0.3 mm was selected due to geometric restrictions; higher displacement values resulted in numerous geometrically infeasible body layer definitions. (One deviation from the high-low values specified in Table I was required for run 4, for which the high value of $r_{2b}=0.66$ mm was not feasible and was thus reduced to 0.54 mm. For this run, proper weighting of the value was taken into consideration when calculating the effects. This modification was deemed to be acceptable since the results showed that overall r_{2b} was insignificant in the measured effects.) Profiles of various geometrically defined models, including the baseline model, are provided in Fig. 2.

C. Computational model

A computational model was used to simulate the flow-induced vibratory motion of a two-dimensional representation of a previously described experimental setup (Drechsel, 2007; Pickup and Thomson, 2009) (see Fig. 3; note the use of symmetry for computational efficiency). The experimental setup consisted of a compressed air source supplying air into a plenum-tube-synthetic vocal fold model series. No vocal tract was included; the supraglottal flow was thus a free jet.

The commercial finite element software ADINA, designed specifically for systems that exhibit fluid-structure interactions and that has been used previously in voice research (e.g., Thomson *et al.*, 2005), was used. The computational model consisted of distinct but fully coupled fluid and solid domains, each of which is described below.

The solid domain included different materials for the model body and cover layers (see Fig. 4). A hyperelastic Ogden material allowed for large strain. The material was defined using linear stress vs strain data over the strain range of interest, with Young's modulus values for the body and cover layers of approximately 15 and 5 kPa, respectively. The density was 1070 kg/m^3 for each layer. Each layer had a Poisson's ratio of 0.495 and a bulk modulus of 10^5 Pa. The Rayleigh damping scheme was used, with damping coefficients of $\alpha=1.948$ and $\beta=2.866\times10^{-4}$. These corresponded to damping ratios of approximately 0.018 and 0.029 at frequencies of 120 and 200 Hz, respectively. A zero-displacement boundary condition was applied to the lateral edge of the solid domain. A fluid-structure interaction boundary condition was applied to the remaining borders of the solid domain (i.e., those that were in contact with the fluid domain). This boundary condition enforced consistent displacement and stress in both fluid and solid domains along the interface.

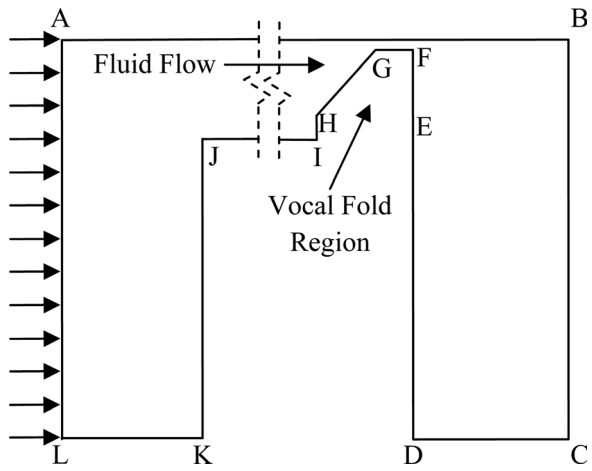

FIG. 3. Computational fluid domain (not to scale). See Table III for geometric and other boundary condition settings. Model is symmetric about line AB.

The fluid (airflow) domain (see Figs. 3 and 4) was governed using the unsteady, viscous, incompressible Navier–Stokes momentum equations coupled with a slightly compressible form of the continuity equation. The air density, viscosity, and bulk modulus values were 1.2 kg/m^3, 1.8×10^{-5} Pa-s, and 1.41×10^5 Pa, respectively. The fluid domain dimensions and boundary conditions are given in Table III. The initial glottal gap width was 0.2 mm.

The slightly compressible fluid model (ADINA, 2009) was used to enable modeling of acoustic feedback in the subglottal section. In the slightly compressible algorithm (Keshtiban *et al.*, 2009), a compressible density, ρ_m, is defined as the incompressible density, ρ, modified by the ratio of pressure, p, to bulk modulus, κ,

$$\rho_m=\rho\left(1+\frac{p}{\kappa}\right). \tag{1}$$

This compressible density replaces the incompressible density in the continuity equation

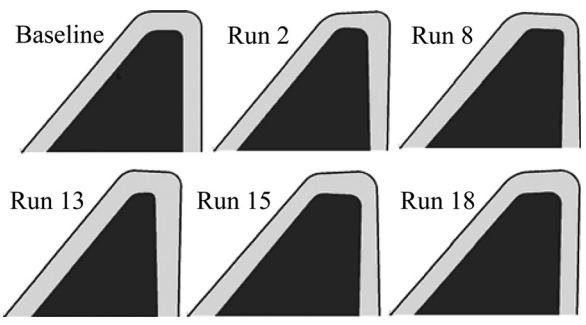

FIG. 2. Illustration of two-layer (cover — gray; body — black) models used in select runs.

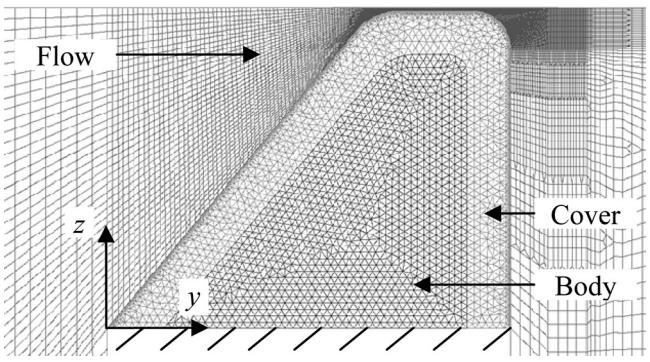

FIG. 4. Meshed solid and fluid domains.

TABLE III. Computational fluid domain line lengths and boundary conditions.

Line segment	Length (m)	Bounday type
AB	0.9767	Slip wall
BC	0.1524	Zero pressure
CD	0.1000	Zero pressure
DE	0.1439	Wall
EF	0.0084	FSI
FG	0.0021	FSI
GH	0.0114	FSI
HI	0.0042	FSI
IJ	0.5588	Wall
JK	0.1397	Wall
KL	0.3080	Wall
AL	0.1524	Fixed pressure (900 Pa)

$$\frac{\rho}{\kappa}\left(\frac{\partial p}{\partial t}+\boldsymbol{v}\cdot\nabla p\right)+\rho_m\nabla\cdot\boldsymbol{v}=0, \tag{2}$$

where t and $\boldsymbol{v}$ denote time and velocity, respectively.

In this formulation, there is no need to use the energy equation. Compared with a fully compressible algorithm, this approach is more computationally efficient, and convergence may be more easily obtained for the low Mach numbers typical of voice production. It is noted that this approach is valid only for $\frac{p}{\kappa}\ll 1$. For these simulations, maximum pressure values were around 3 kPa, for maximum $\frac{p}{\kappa}$ ratios of around 0.02, thus satisfying the $\frac{p}{\kappa}\ll 1$ condition.

Figure 4 shows the meshes in both domains. Model verification was performed to ensure that the solution was reasonably independent of mesh density and time step size. The fluid domain utilized primarily four-node quadrilateral elements and consisted of approximately 19 000 nodes. The solid domain used three-node triangular elements and contained approximately 3000 nodes. The time step size was 1.25×10^{-5} s. As has been done previously (Thomson *et al.*, 2005), a contact line was used to prevent complete fluid domain mesh collapse as the solid domain moved medially. This contact line was placed such that the minimum allowable glottal gap width was 0.05 mm.

D. Yield calculation

To estimate the effect of each of the 13 geometric parameters on the model's response, various output measures, denoted here as yields, were obtained. These included the following (described in detail below; see also Table IV): flow-induced vibration frequency (f_{FIV}), changes in lateral glottal width (Δd), flow rate (Δq), intraglottal angle ($\Delta\alpha$), and lateral phase delay ($\Delta\varphi/T$, where T is the vertical glottal thickness). Similar measures of lateral phase delay were previously used by Titze *et al.* (1993) and Boessenecker *et al.* (2007) to quantify mucosal wave-like motion.

TABLE IV. Nomenclature of measured yields.

Yield	Definition
f_{FIV} (Hz)	Flow-induced vibration frequency
Δd (mm)	Difference between min/max glottal width
Δq (m^3/s)	Difference between min/max flow rate
$\Delta\alpha$ (°)	Difference between min/max intraglottal angle
$\Delta\phi/T$(°/mm)	Lateral phase delay between points near entrance and exit radii
f_{MOD} (Hz)	Second modal frequency

These five yields were calculated for each case after steady-state oscillation was reached. The flow-induced vibration frequency (f_{FIV}) was measured by tracking the "entrance point" position (see Fig. 1). Measures of Δd, Δq, $\Delta\alpha$, and $\Delta\varphi/T$ are visually portrayed in Fig. 5, in which three different simulation results are shown. The difference in minimal glottal width (Δd) was measured by taking the net difference between high and low values of the minimum glottal gap (z-direction; see coordinate system in Fig. 4) over time. The change in flow rate (Δq) was measured by integrating the velocity profile just downstream of the model, multiplying by 0.017 cm (close to the length of the average adult male's vocal folds, Titze, 2006), and taking the difference between high and low flow rates over time. The change in intraglottal angle ($\Delta\alpha$) was defined by tracking the y- and z-locations of the entrance and exit points and taking the net difference between the low and high angle between them. It is noted that this is only an approximation, since during vibration the glottal surface deformed and was thus not linear. The phase delay ($\Delta\varphi/T$) was measured by tracking the entrance and exit points' z-locations over time, taking the difference in time between peak values, dividing by the period, multiplying by 360°, and dividing by the vertical glottal thickness (T).

The effect of each parameter was calculated as follows. Each parameter's yields from runs with a specified "high" value were averaged. Each parameter's yields from runs with a specified "low" value were also averaged, subtracted from the "high" yield average, and then normalized. A resulting value relatively close to zero indicated that even though the parameter levels may have been changing, the overall yield did not vary; i.e., the parameter had minimal effect on model response. A value close to +1 or −1 meant that a particular parameter had a high impact on the measured yield. A positive effect meant that increasing that parameter's value increased the yield, while a negative effect meant the opposite.

Statistical p-values were estimated for each parameter at each measured yield using the statistical software package JMP (SAS Institute, Inc., Cary, NC). A standard $\alpha=0.05$ value was used. Since there was no anticipated variation in the calculated yields (due to the use of computational analysis), a Monte Carlo technique was used to provide a pseudo-standard error (PSE) which allowed for calculated p-values. p-values less than 0.05 were considered to be significant; p-values less than 0.10 but greater than 0.05 were considered to be marginally significant.

In addition to these yields, animations of the simulated model motion were created for visual inspection. Finally, *in vacuo* modal analysis was performed on each model (also using ADINA). These modal analysis results were not used to estimate which parameters were important in governing the

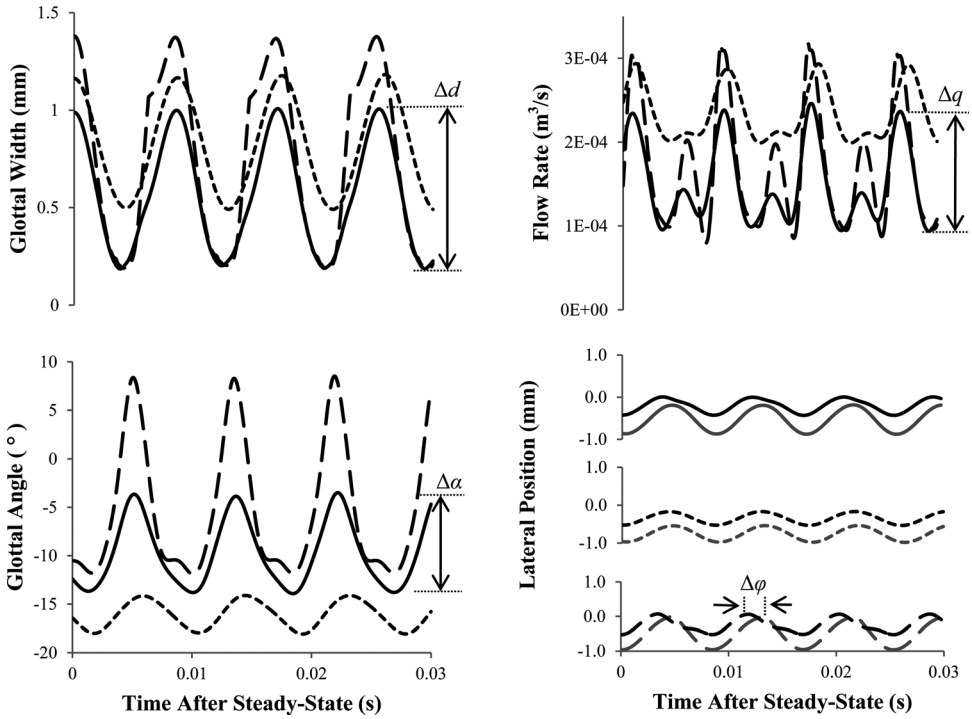

FIG. 5. Predicted yields for the baseline (solid), run 13 (short dashes), and run 18 (long dashes) models. In the lower right plot, black and gray colors denote entrance and exit point positions, respectively (see Fig. 1).

flow-induced vibration characteristics but were used to assist in interpreting the results. As discussed below, the second modal frequency, f_{MOD}, was of particular interest.

III. RESULTS AND DISCUSSION

Table V lists the six calculated yields from each run, and Fig. 6 contains plots of the normalized effects of each parameter per yield, with significant and marginally significant p-values denoted.

TABLE V. Yield values for each run.

Run	f_{FIV} (Hz)	Δd (mm)	Δq (m^3/s)	$\Delta\alpha$ (°)	$\Delta\phi/T$ (°/mm)	f_{MOD} (Hz)
0	117.8	0.829	1.53E-04	10.5	18.5	116.8
1	119.2	1.045	1.89E-04	15.2	24.9	120.4
2	115.9	1.264	2.40E-04	20.0	26.2	114.9
3	121.3	0.724	1.17E-04	7.1	14.4	122.6
4	114.5	1.120	2.01E-04	10.5	17.5	115.1
5	118.2	0.715	1.31E-04	10.4	16.7	119.1
6	118.8	1.023	2.01E-04	16.7	28.6	117.0
7	119.1	0.757	1.53E-04	13.2	21.2	119.9
8	121.5	0.503	0.92E-04	7.3	18.0	120.7
9	116.2	0.732	1.01E-04	4.5	8.5	114.1
10	117.8	0.694	1.96E-04	12.7	21.7	117.0
11	120.0	1.061	1.96E-04	16.0	26.6	121.1
12	113.8	1.223	2.17E-04	16.3	20.8	114.6
13	115.2	0.712	0.98E-04	4.1	8.1	112.1
14	115.9	1.040	1.91E-04	11.0	19.4	115.6
15	122.3	1.099	2.48E-04	19.7	32.5	119.4
16	118.6	0.861	1.62E-04	9.7	16.2	118.4
17	117.5	0.733	1.29E-04	7.3	13.0	115.2
18	118.8	1.202	2.38E-04	20.6	30.3	117.5
19	116.1	1.253	2.54E-04	20.0	28.7	114.1
20	119.3	0.711	1.07E-04	6.0	9.3	119.4

A. Flow-induced vibration frequency and profiles

The flow-induced vibration frequency (f_{FIV}) ranged from 113 to 122 Hz, which is within the typical range of male phonation. The parameter that had the largest effect on f_{FIV} was the cover layer superior angle (θ_{3c}), which had a negative effect. Other significant parameters were the body layer superior angle (θ_{3b}) and the cover exit radius (r_{2c}), both of which had positive effects. Marginally significant parameters were θ_{2c}, T, and X18 (an unknown interaction).

The flow-induced vibration profiles from three runs through one cycle of vibration are illustrated in Fig. 7. Cases displayed include the baseline model (run 0) and runs 13 and 18. For the baseline model, the cover and body layer pre-phonatory intraglottal angles were 0°. Its movement was similar to previous similarly defined synthetic models (e.g., Pickup and Thomson, 2010). The vibration frequency was 117 Hz. There was minimal presence of mucosal wave-like motion, and the glottal profile stayed primarily divergent throughout the cycle (this is also evident in Fig. 5). Run 13 produced similar results as the baseline model, with no evidence of mucosal wave-like motion and consistently divergent glottal profile throughout the cycle. Its cover layer intraglottal angle (θ_{2c}) was assigned its low value of −2.75° (divergent). As seen in Figs. 5 and 7, run 18 showed improvement in motion over that of both the run 0 and run 13 models, in that the intraglottal angle alternated between a convergent profile during opening and a divergent profile during closing. A common feature between run 18 and other cases with similar convergent-divergent motion was that the cover layer intraglottal angle (θ_{2c}) was set to its high value of 2.75° (convergent).

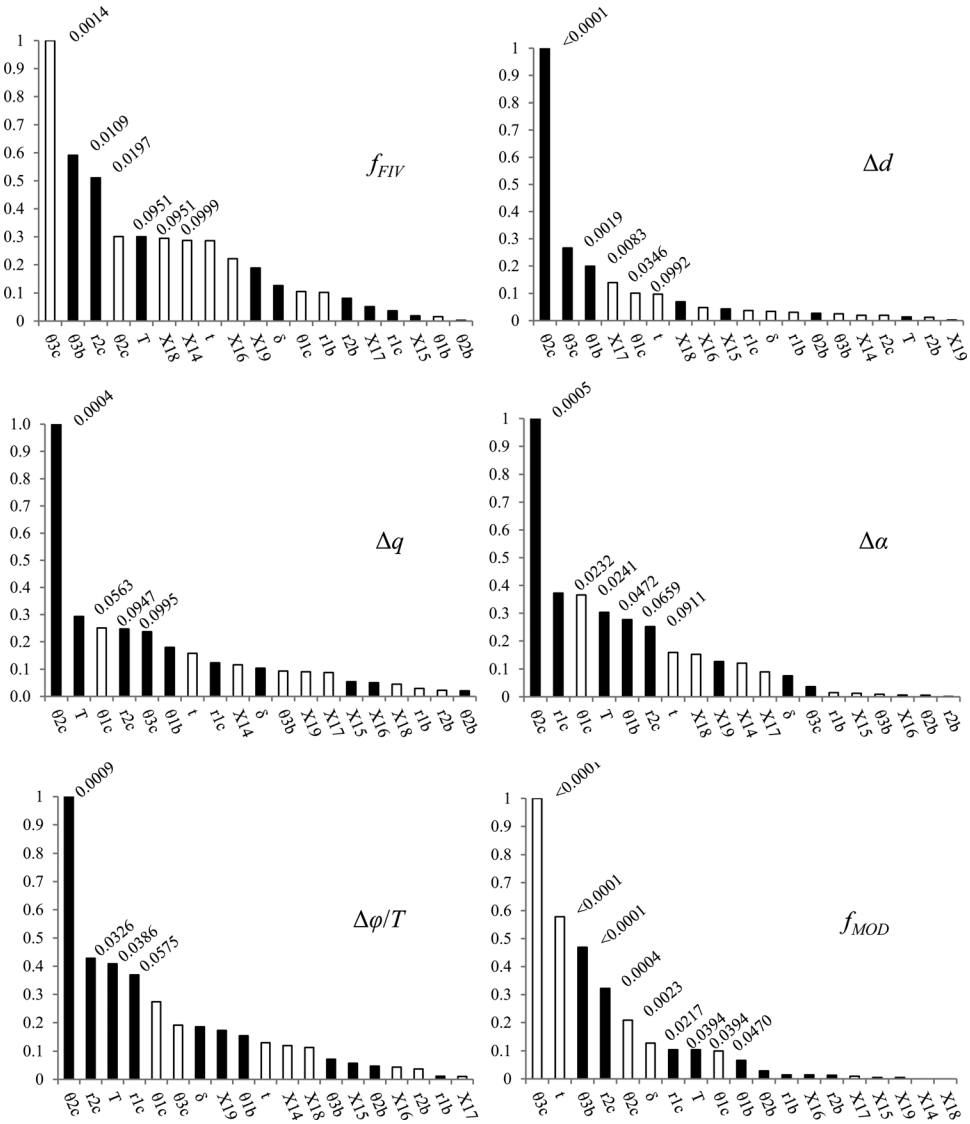

FIG. 6. Normalized yield effects: flow-induced vibration frequency (f_{FIV}), change in glottal width (Δd), change in flow rate (Δq), change in intraglottal angle ($\Delta\alpha$), lateral phase delay ($\Delta\varphi/T$), and second *in vacuo* modal vibration frequency (f_{MOD}). Filled bars represent positive effects; empty bars represent negative effects. Numbers above bars represent individual p-values.

The significance of the cover superior angle (θ_{3c}) in influencing f_{FIV} may be related to its role in governing model stiffness. The first three *in vacuo* mode shapes for run 18 are shown in Fig. 8. The first mode featured primarily inferior–superior motion. The second and third modes featured combined medial-lateral and convergent-divergent motion. The second mode's convergent profile occurred as it was laterally displaced, whereas the divergent profile occurred as it was medially displaced. The third mode shape exhibited the opposed trend. The first and third modal frequencies were around 50 and 140 Hz, respectively, whereas the second modal frequencies (f_{MOD}) were very close to those of the

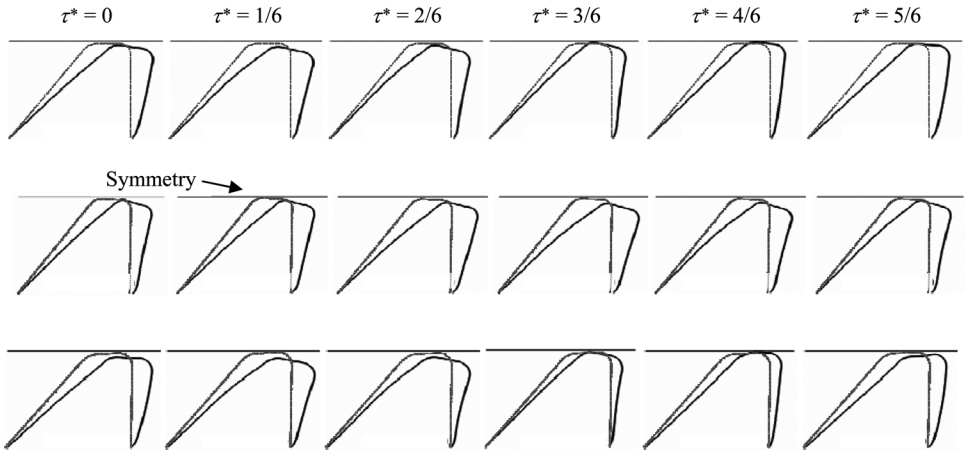

FIG. 7. Profiles of different parametric models over one oscillation cycle. Phase relative to fraction of one cycle (τ^*) denoted. The baseline model (run 0, top row), run 13 (middle row), and run 18 (bottom row) are all shown. Gray profiles represent each model's original position.

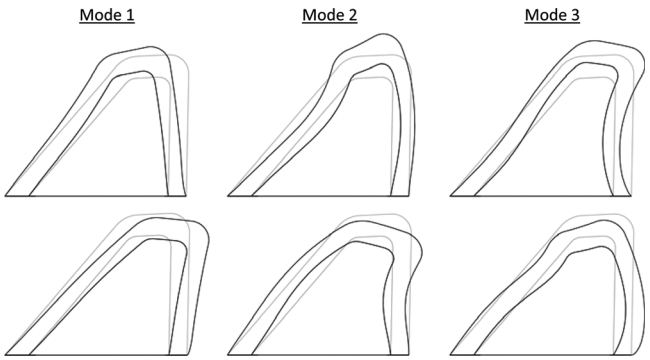

FIG. 8. Mode shapes 1 through 3. Light gray lines denote undeformed shapes.

flow-induced vibration frequency. This is evident in Fig. 9, in which a good correlation ($R^2 = 0.75$) between f_{FIV} and f_{MOD} is seen. Weaker correlations were found between f_{FIV} and the first and third modal frequencies ($R^2 = 0.62$ and 0.23, respectively). The somewhat stronger correlation between f_{FIV} and f_{MOD} is possibly due to acoustic coupling of the subglottal system with the model's second mode of vibration (Zhang *et al.* 2006b, 2009). As seen in Fig. 6, the second mode of vibration (f_{MOD}) was most influenced by θ_{3c} the same parameter that most significantly influenced f_{FIV}. Decreasing θ_{3c} led to a larger inferior–superior base length, which in turn increased the model's effective stiffness. This caused f_{MOD} to increase, and possibly by virtue of the acoustic coupling, f_{FIV} to increase, although as explained below, further studies would be needed to test this hypothesis.

For comparison, the expected resonance frequency of the subglottal section is here estimated. If only the straight subglottal tube (section JI, length 0.5588 m, see Fig. 3 and Table III) is considered, the quarter-wavelength resonance frequency is 153 Hz (based on a speed of sound of 343 m/s). If the plenum is also considered, the overall length increases to 0.8668 m, and the quarter-wavelength resonance frequency decreases to 98.9 Hz. To more closely estimate the fundamental resonance frequency of the subglottal section, further simulations were performed as follows. The inlet boundary condition was changed from a constant 900 Pa pressure to a pure sine wave with an amplitude of 100 Pa. This resulted in a temporally varying pressure fluctuation (that included acoustic reflections) within the subglottal section. Simulations were performed with input frequencies ranging from 100 to 150 Hz in 10 Hz increments, with one additional simulation at 135 Hz. A somewhat coarser grid and a larger time step size were used since small scale flow motion was not the object of these simulations. As the input frequency approached resonance, the maximum pressure within the fluid domain increased, as can be seen in Fig. 10. In this figure, a maximum pressure around 135 Hz is evident, which is in between the above-estimated quarter-wavelength resonant frequencies and which is also not far from the flow-induced vibration frequencies (see Fig. 9 and Table V).

To visualize the acoustic fluctuations, as well as the temporal relationship between pressure and model motion, pressure waveforms at three different locations (subglottal, glottal, and supraglottal) are shown in Fig. 11, along with glottal width vs time. Also shown is the pressure along the symmetry line at four instances of time of one oscillation cycle. Note that location y1 in Fig. 11 is near the subglottal microphone position in the synthetic vocal fold model experiments reported by Thomson *et al.* (2005). The pressure waveform predicted by the present simulations at location y1 (approximately sinusoidal with a mean of 900 Pa and an amplitude of about 835 Pa) is similar to that reported by Thomson *et al.* (2005) (also approximately sinusoidal, with a mean of 2000 Pa and an amplitude of approximately 1200 Pa; the differences in magnitude here attributed to different subglottic lengths, different material properties, and a three-dimensional physical model vs a two-dimensional simulation). The subglottic acoustic pressure fluctuation seen in

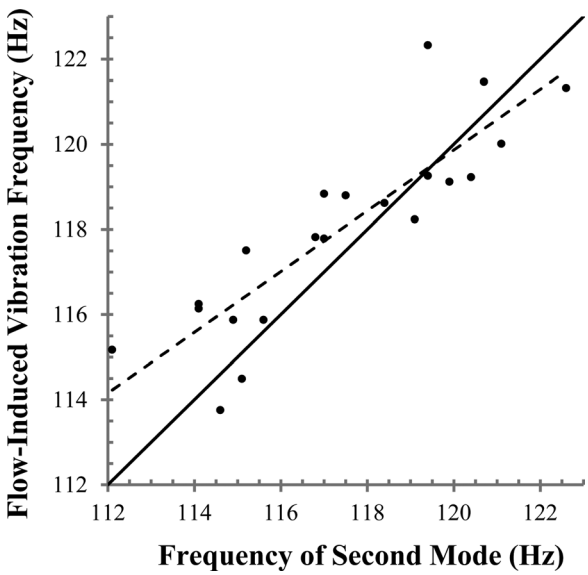

FIG. 9. Relationship between flow-induced vibration frequency (f_{FIV}) and the second modal frequency (f_{MOD}) of the solid models. Hypothetical one-to-one relationship (solid line) and actual data trend line (dashed line, $R^2 = 0.75$) are shown.

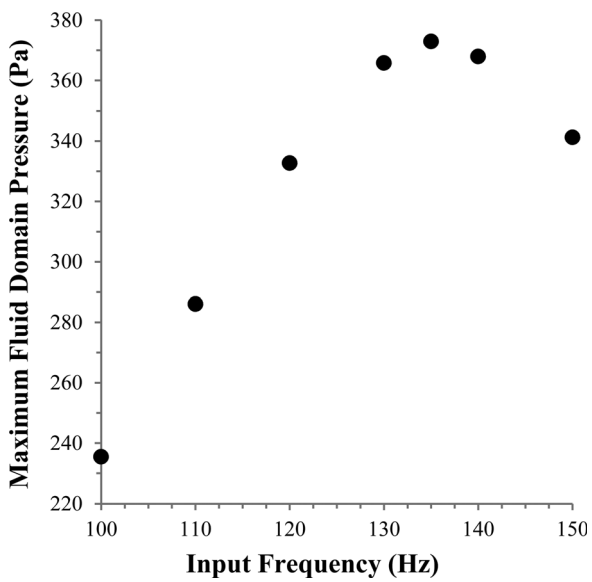

FIG. 10. Predicted maximum pressure in the fluid domain vs frequency, for the simulations in which a sinusoidal inlet pressure was prescribed.

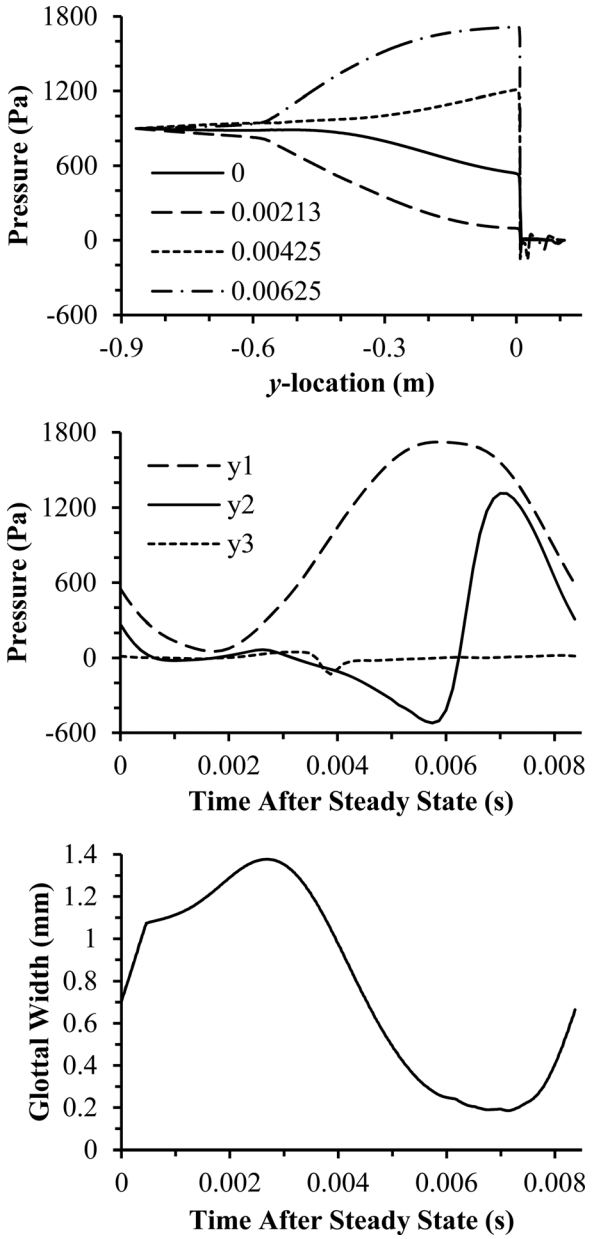

FIG. 11. Pressure and displacement data for run 18. *Top*: Pressure along the symmetry line (line AB, Fig. 3) vs streamwise location at four time instances of one cycle after reaching steady-state, as denoted in legend. *Middle:* Pressure vs time at three streamwise locations on the symmetry line, with y1 = −0.0212 m (subglottis), y2 = 0.00919 m (intraglottis), and y3 = 0.02 m (supraglottis); see the coordinate system in Fig. 4. *Bottom:* Glottal width vs time.

Fig. 11 is similar to what one would expect in a quarter-wavelength resonator.

Considering these data and observations, as well as the results of other studies of subglottal acoustic coupling with a similar synthetic model (Zhang *et al*., 2006a, b, 2009), it is very likely that subglottal acoustic coupling played a significant role in governing the present model's vibration. The precise coupling mechanism is not immediately evident, however. Above it was suggested that coupling with the second mode may have occurred; however, another possible explanation is that the oscillations resulted from aeroelastic eigenmode synchronization (e.g., Zhang, 2008, 2009). Further work would be needed to identify the nature of the acoustic-aerodynamic coupling of this model.

B. Glottal width, flow rate, intraglottal angle, and phase delay

The other four measured yields (change in glottal width, Δd; change in flow rate, Δq; change in intraglottal angle, $\Delta\alpha$; and phase delay, $\Delta\varphi/T$) all exhibited somewhat similar trends in terms of significant parameters. All were more strongly influenced by the cover intraglottal angle (θ_{2c}) than by any other yield.

The glottal width (Δd) was mainly influenced by θ_{2c}, which had a positive effect. The largest differences in the glottal width were around 1.26 mm, compared with around 4 mm previously measured using excised human hemilarynges (Doellinger and Berry, 2006; Boessenecker *et al*., 2007). Only one body layer geometry (θ_{1b}) had a significant effect on Δd. Other significant parameters included θ_{3c} and X17, with marginal significance from θ_{1c}.

Unknown interactions of parameters appear to be somewhat significant only in Δd and f_{FIV} yields. As mentioned above, the Plackett–Burman design has interactions confounded in the main effects. In order to understand the magnitude of the effect that interactions play in governing f_{FIV} and Δd, further parametric studies considering the most influential parameters and their interactions would be necessary.

The change in flow rate (Δq) was mainly influenced by θ_{2c} (positive effect). Other parameters that affected Δq were T, θ_{1c}, and r_{2c}. This is important since changes in flow rate are strongly correlated with sound production. The change in intraglottal angle ($\Delta\alpha$) was also primarily positively influenced by θ_{2c}. Other parameters that effected $\Delta\alpha$ include r_{1c}, θ_{1c}, T, θ_{1b}, and r_{2c}. Adjusting these parameters for large $\Delta\alpha$ is desirable for generating alternating convergent-divergent motion. For phase delay, other significant and marginally significant parameters included r_{2c}, T, and r_{1c}. All of these geometries had a positive effect. Relative to the baseline model, increased phase delays are desirable; hence, increased values of θ_{2c} (more convergent profile), r_{2c}, T, and r_{1c} are recommended for improving phase delay. Further refined sensitivity studies would be helpful in elucidating the precise roles played by the significant parameters in governing model motion.

C. Overall parameter significance

To quantify the overall effect of each parameter on model movement, the geometric parameters for Δd, Δq, $\Delta\alpha$, and $\Delta\varphi/T$ were ranked for each yield (i.e., assigned a number 1–19), summed, and normalized. These overall rankings are shown in Fig. 12 to provide a graphical representation of the parameters that exerted the greatest overall effect on model motion. The cover medial angle profile θ_{2c} was clearly the most significant factor overall. It had the greatest effect (positive) on all calculated yields, except for the flow-induced vibration and second modal frequencies. Consistent with the hypothesis of Pickup and Thomson (2010) (see Introduction), altering the intraglottal angle to have a convergent prephonatory profile significantly improved model motion in terms of generating alternating convergent-divergent motion and mucosal wave-like motion (phase delay). The influence

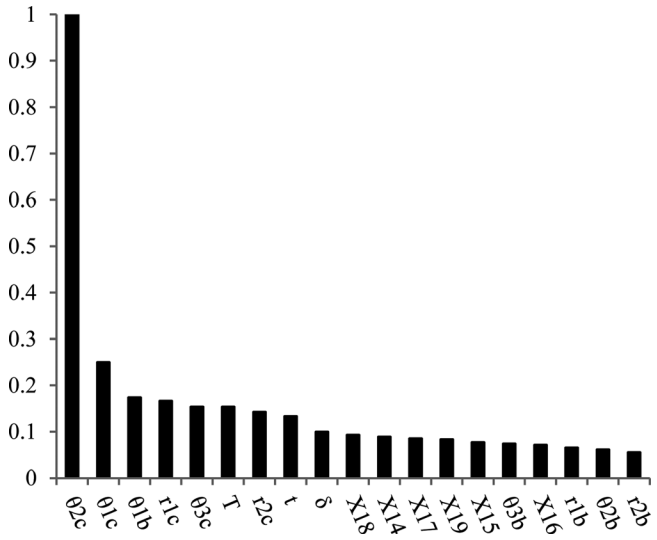

FIG. 12. Normalized summed effects for Δd, Δq, $\Delta\alpha$, and $\Delta\varphi/T$.

of θ_{2c} is followed by θ_{1c}, θ_{1b}, r_{1c}, θ_{3c}, T, r_{2c} (all of which, except for θ_{1b}, govern the cover layer profile), δ and t (which govern cover layer thickness), and other interactions and body layer geometries.

The other two model cover layer angles (θ_{1c} and θ_{3c}) also had an effect on model motion, though not nearly as profound as θ_{2c}. θ_{1c} had a negative effect on calculated yields, including Δq, $\Delta\alpha$, and $\Delta\varphi/T$. θ_{3c} had a positive effect on Δd and negative effect on f_{FIV} and f_{MOD}.

The entrance and exit radii (r_{1c} and r_{2c}) showed similar effects on all six yields. Increasing either would provide an increase in Δq, $\Delta\alpha$, and $\Delta\varphi/T$. Since large glottal angle differences and changes in flow rate are desirable for improving the motion and increasing sound production, relatively larger leading and trailing edge radii may be advisable.

Another somewhat influential geometric feature was the glottal thickness (T), which had a significant or marginally significant positive effect on Δq, $\Delta\alpha$, and $\Delta\varphi/T$. Increasing T had a significant impact on the phase difference between the inferior–superior portions of the glottis (similar to θ_{2c}), suggesting that increasing T may provide improved mucosal wave-like motion for physical modeling.

It is interesting to note that three of the body dimensions r_{1b}, θ_{2b}, r_{2b} did not have a major effect on any of the measured yields. Two body dimensions affected the measured yields: θ_{1b}, which had a positive effect on Δd and $\Delta\alpha$, and θ_{3b}, which had a positive effect on f_{FIV} and $\Delta\alpha$. Some of the unknown interactions had higher overall significance than several body parameters. Therefore, the interactions of the cover layer geometries, θ_{1b}, and θ_{3b} may be important to model motion and should be investigated.

D. Additional model considerations

As mentioned in the Introduction, one of the primary motivations for the present study was to investigate the role of geometric features on the motion of a previously used synthetic vocal fold model in order to improve its motion. The results showed that improvements to model motion could be achieved by changing specific parameters; however, it is evident that further advances need to be made in order to yield a synthetic model that exhibits more life-like motion. The following paragraphs include specific recommendations for further model advances and studies.

The synthetic model that formed the basis for the present work has been shown to couple with subglottal acoustics (Zhang *et al.*, 2006b, using a one-layer model, and Drechsel, 2007, using a two-layer model). However, the vocal folds do not seem to exhibit significant subglottal acoustic coupling. It will therefore be important for future synthetic models to exhibit weaker coupling with subglottal acoustics. Zhang *et al.* (2006b) showed that when placing vertical restraints on a one-layer synthetic model, the model vibrated in response to aerodynamic rather than acoustic coupling. Zhang *et al.* (2009) further showed that aerodynamic coupling could also be achieved by reducing the stiffness of a one-layer model. It is therefore likely that a two-layer model with a much more flexible cover layer, possibly combined with a stiffer body layer than what was used in the presently described work, will yield the desired results in terms of reduced subglottal acoustic coupling. It is also likely that such a model will exhibit the added beneficial feature of reduced inferior–superior displacement during vibration.

Another consideration is that of the model baseline configuration regarding both geometry and stiffness. The geometry considered here is an idealization of that of the vocal folds. The conclusions reached here regarding parameter significance may or may not apply to a model with a different baseline geometry, such as that described by Sidlof *et al.* (2008). The same may be said if different body-cover stiffness ratios were to be implemented. For example, a much more flexible cover would be expected to exhibit much larger deformation, potentially altering the relative significance of geometric factors. Alternatively, a very stiff body may more significantly increase the relative importance of body dimensions. It is recommended that such geometric and material considerations should be explored in the future using self-oscillating models.

Additional insight could also be obtained by further investigation of geometric parameters. In the above sections, parameters that were significant in governing the model's vibration were identified. However, the current approach does not allow for the magnitude of each parameter's influence on model vibration, i.e., the sensitivity of model motion to each parameter's variation, to be quantified. It also includes only very limited consideration of the interactions between parameters. Determination of these effects can be done via future systematic parametric variation and sensitivity analysis. Furthermore, investigation of numerous additional model parameters, such as model depth, prephonatory glottal width, anterior–posterior geometric parameters, material stress-strain nonlinearity, and material anisotropy, may yield important physical insight.

IV. CONCLUSIONS

In this paper, the influence of geometric parameters on the flow-induced vibratory response of a simplified vocal

fold model is discussed. It is shown that this model may be altered geometrically for more favorable (realistic) model movement, although further improvements are still needed.

Prior research has shown that the intraglottal angle, vocal fold depth, and vocal fold length significantly influence vocal fold model motion (Cook and Mongeau, 2007; Zhang, 2009). The present work considers more geometric attributes of a simplified model and shows that the geometric parameters that play the most important role in affecting the flow-induced vibration frequency, second modal frequency, phase delay, change in glottal angle during phonation, glottal area, and flow rate are the cover layer geometries (foremost, the intraglottal cover layer angle, θ_{2c}, followed by θ_{1c}, r_{1c}, θ_{3c}, T, r_{2c}, and t), and the inferior and superior glottal angles of the body (θ_{1b} and θ_{3b}).

A key aspect of vocal fold movement is the mucosal wave. Previous geometrically simplified synthetic models have not displayed this type of motion. The phase delay measurements here provided a quantitative assessment of model mucosal wave-like motion; the phase delays calculated in this work are similar to data obtained using excised human larynges (Boessenecker *et al.*, 2007). Although an optimized model was not created in this study, the results (see Table V) show the potential for creating a model that has at least a 32.5°/mm phase delay (lateral $\Delta\varphi$ values calculated by Boessenecker *et al.* reached a maximum of 89°, which corresponds to a $\Delta\varphi/T$ value of approximately 44.5°/mm). Therefore, previously limited mucosal wave-like features on simplified models may be obtainable if these geometric definitions of the cover layer are incorporated. Further, the present work shows that using a convergent profile will increase intraglottal phase delays and alternating convergent-divergent glottal angles toward a more accurate simulation of human vocal fold movement.

The results from this design-of-experiment study do not reflect the level of influence of each parameter in its entirety. Therefore, recommended future work includes a full-factorial statistical analysis using the subset of significant parameters identified in this study. This will provide information on the interaction of significant parameters. Also, it would be beneficial to perform physical tests on synthetic simplified models with improved geometric features suggested above to validate the computational results. Such analysis and testing is suggested so that specific geometric values for each parameter may be recommended. Further studies over a wider range of parameter values, including three-dimensional geometric parameters, and exploration and development of anisotropic modeling materials and models with reduced subglottal acoustic coupling are also strongly recommended.

Finally, it is here stressed that these results are applicable to the two-layer vocal fold models referenced herein, which are clearly simplified representations of the human vocal folds. Because of differences between these models and the human vocal folds (e.g., material stiffness, material anisotropy, geometry, and weaker acoustic coupling in the human case), the results of the present study may not necessarily directly apply to human vocal fold vibration. Consequently, the primary utility of these results lies in contributing toward the development of synthetic (and possibly computational) models with more realistic life-like motion, rather than conclusions regarding the role of geometry on human vocal fold vibration. Regarding the latter issue, however, the methodology used in the present study may be useful in future studies aimed at exploring the influence of specific vocal fold geometric features on human phonation.

ACKNOWLEDGMENTS

This work was supported by Grant R01 DC005788 from the National Institute on Deafness and Other Communication Disorders (Dr. Luc Mongeau, PI; Subcontract to Brigham Young University through McGill University).

ADINA (**2009**). ADINA Theory and Modeling Guide Vol. III: ADINA CFD & FSI, (ADINA R&D, Inc.), pp. 35–36.

Agarwal, M., Scherer, R. C., and Hollien, H. (**2003**). "The false vocal folds: Shape and size in frontal view during phonation based on laminagraphic tracings," J. Voice **17**, 97–113.

Becker, S., Kniesburges, S., Muller, S., Delgado, A., Link, G., Kaltenbacher, M., and Dollinger, M. (**2009**). "Flow-structure-acoustic interaction in a human voice model," J. Acoust. Soc. Am. **125**(3), 1351–1361.

Bless, D., Hirano, M., and Feder, R. (**1987**). "Videostroboscopic evaluation of the larynx," Ear Nose Throat J. **66**, 289–296.

Boessenecker, A., Berry, D. A., Lohscheller, J., Eysholdt, U., and Doellinger, M. (**2007**). "Mucosal wave properties of a human vocal fold," Acta Acust. Acust. **93**, 815–823.

Chan, R. W., Titze, I. R., and Titze, M. R. (**1997**). "Further studies of phonation threshold pressure in a physical model of the vocal fold mucosa," J. Acoust. Soc. Am. **101**(6), 3722–3727.

Cook, D. D., and Mongeau, L. (**2007**). "Sensitivity of a continuum vocal fold model to geometric parameters, constraints, and boundary conditions," J. Acoust. Soc. Am. **121**(4), 2247–2253.

Cook, D. D., Nauman, E., and Mongeau, L. (**2009**). "Ranking vocal fold model parameters by their influence on modal frequencies," J. Acoust. Soc. Am. **126**(4), 2002–2010.

Doellinger, M., and Berry, D. A. (**2006**). "Visualization and quantification of the medial surface dynamics of an excised human vocal fold during phonation," J. Voice **20**(3), 401–413.

Drechsel, J. S. (**2007**). "Characterization of synthetic self-oscillating vocal fold models," M.S. Thesis, Brigham Young University, Provo, Utah.

Drechsel, J. S., and Thomson, S. L. (**2008**). "Influence of supraglottal structures on the glottal jet exiting a two-layer synthetic, self-oscillating vocal fold model," J. Acoust. Soc. Am. **123**(6), 4434–4445.

Keshtiban, I., Belblidia, F., and Webster, M. (**2009**). "*Compressible Flow Solvers for Low Mach Number Flows—A Review*," Institute of Non-Newtonian Fluid Mechanics, Department of Computer Science, University of Wales, Swansea, SA2 8PP, UK.

Lawson, J., and Erjavec, J. (**2001**). *Modern Statistics for Engineering and Quality Improvement*, 1st ed. (Wadsworth Group, Duxbury, Pacific Grove, CA), p. 759.

Li, S., Scherer, R. C., Wan, M., Wang, S., and Wu, H. (**2006**). "Numerical study of the effects of inferior and superior vocal fold surface angles on vocal fold pressure distributions," J. Acoust. Soc. Am. **119**(5), 3003–3010.

Misun, V., Svancara, P., and Vasek, M. (**2011**). "Experimental analysis of the characteristics of artificial vocal folds," J. Voice (in press).

Nanayakkara, I. (**2005**). "Vocal fold superior and inferior angles measured from radiographic images," M.S. Thesis, Bowling Green State University, Bowling Green, OH.

Neubauer, J., Zhang, Z., Miraghaie, R., and Berry, D. A. (**2007**). "Coherent structures of the near field flow in a self-oscillating physical model of the vocal folds," J. Acoust. Soc. Am. **121**(2), 1102–1118.

Pickup, B. A., and Thomson, S. L. (**2009**). "Influence of asymmetric stiffness on the structural and aerodynamic response of synthetic vocal fold models," J. Biomech. **42**, 2219–2225.

Pickup, B. A., and Thomson, S. L. (**2010**). "Flow-induced vibratory response of idealized vs. magnetic resonance imaging-based synthetic vocal fold models," J. Acoust. Soc. Am. **128**(3), EL124–EL129.

Scherer, R. C., Shinwari, D., De Witt, K. J., Zhang, C., Kucinschi, B. R., and Afjeh, A. A. (**2001a**). "Intraglottal pressure profiles for a symmetric

and oblique glottis with a divergence angle of 10 degrees," J. Acoust. Soc. Am. **109**(4), 1616–1630.
Scherer, R. C., De Witt, K. J., and Kucinschi, B. R. (**2001b**). "The effect of exit radii on intraglottal pressure distributions in the convergent glottis," J. Acoust. Soc. Am. **110**(5), 2267–2269.
Sidlof, P., Svec, J. G., Horacek, J., Vesely, J., Klepacek, I., and Havlik, R. (**2008**). "Geometry of human vocal folds and glottal channel for mathematical and biomechanical modeling of voice production," J. Biomech. **41**(5), 985–995.
Stiblar-Martincic, D. (**1997**). "Histology of laryngeal mucosa," Acta Otolaryngol. **527**, 138–141.
Tayama, N., Chan, R., Kaga, K., and Titze, I. R. (**2002**). "Functional definitions of vocal fold geometry for laryngeal biomechanical modeling," Ann. Otol. Rhinol. Laryngol. **111**, 83–92.
Thomson, S. L., Mongeau, L., and Frankel, S. H. (**2005**). "Aerodynamic transfer of energy to the vocal folds," J. Acoust. Soc. Am. **118**(3), 1689–1700.
Titze, I. R. (**2006**). *The Myoelastic Aerodynamic Theory of Phonation* (National Center for Voice and Speech, Iowa City, Iowa), p. 19.
Titze, I. R., Jiang, J. J., and Hsiao, T. (**1993**). "Measurement of mucosal wave propagation and vertical phase difference in vocal fold vibration," Ann. Otol. Rhinol. Laryngol. **102**, 58–63.
Titze, I. R., Schmidt, S. S., and Titze, M. R. (**1995**). "Phonation threshold pressure in a physical model of the vocal fold mucosa," J. Acoust. Soc. Am. **97**(5), 3080–3084.
Zhang, Z. (**2008**). "Influence of flow separation location on phonation onset," J. Acoust. Soc. Am. **124**(3), 1689–1694.
Zhang, Z. (**2009**). "Characteristics of phonation onset in a two-layer vocal fold model," J. Acoust. Soc. Am. **125**(2), 1091–1102.
Zhang, Z., Neubauer, J., and Berry, D. A. (**2006a**). "The influence of subglottal acoustics on laboratory models of phonation," J. Acoust. Soc. Am. **120**(3), 1558–1569.
Zhang, Z., Neubauer, J., and Berry, D. A. (**2006b**). "Aerodynamically and acoustically driven modes of vibration in a physical model of the vocal folds," J. Acoust. Soc. Am. **120**(5), 2841–2849.
Zhang, Z., Neubauer, J., and Berry, D. A. (**2009**). "Influence of vocal fold stiffness and acoustic loading on flow-induced vibration of a single-layer vocal fold model," J. Sound Vib. **322**, 299–313.